Composites: Part A 185 (2024) 108288

Contents lists available at ScienceDirect

Composites Part A

journal homepage: www.elsevier.com/locate/compositesa

Limitations of composite strength theory for predicting the ultimate strengths of layered 3D printing polymers

Gonghe Zhang [a], Xiaodong Zheng [a], Qinglin Wang [a], Yinxu Ni [b], Fenghua Liu [b], Kai Zhao [c], Luoyu Roy Xu [a,*]

[a] School of Mechanical Engineering and Mechanics, MOE Key Laboratory of Impact and Safety Engineering, Ningbo University, Ningbo, Zhejiang 315211, China
[b] Zhejiang Key Laboratory of Additive Manufacturing Materials, Ningbo Institute of Materials Technology and Engineering, Chinese Academy of Science, Ningbo, Zhejiang 315211, China
[c] Structural Composites LLC, Houston, TX 77055, USA

ARTICLE INFO

Keywords:
A. Layered structure
B. Strength
C. Mechanical testing
D. 3D printing

ABSTRACT

Composite laminates and 3D printing materials both have layered structures. Although the Tsai–Hill composite strength criterion is useful for predicting the strengths of some 3D printing polymers made with fused filament fabrication (FFF), our experimental and theoretical studies showed that this criterion has some limitations in predicting the strengths of other 3D printing polymers. In this study, a new quadratic strength criterion was employed to predict a conservative lower bound for the strengths of polymers made with FFF and selective laser sintering (SLS). The printing surface angles of the printing specimens ranged from 0° to 90°. Interestingly, the scope of this study unexpectedly widened from strength research to fracture mechanics research because dynamic crack branching was observed in some SLS specimens (printing surface angles ranged from 0° to 75°) under static tension—a novel phenomenon among 3D printing materials. Crack branching not only followed previous crack branching rules, such as rules on the crack speed and energy release but also presented new challenges for dynamic fracture mechanics theory.

1. Introduction

Because more and more 3D printing materials are being used in load-bearing structures, their mechanical properties are being extensively studied. The earliest 3D printing materials made with fused filament fabrication (FFF) were the first used for mechanical property research. The FFF method shown in Fig. 1 uses numerous rasters and layers that can be printed in different directions [1]. Some researchers have employed fiber-reinforced composite mechanics to characterize these layered materials since rasters and fibers have a certain similarity and both material systems are layered. Furthermore, researchers have also used the laminate theory of composite materials directly to predict the stiffness and strength of FFF polymers without any modification. However, this approach has significant limitations because other 3D printing techniques do not employ rasters. Composite laminates and general 3D printing materials mainly have the similar layered structures. Fig. 1 also illustrates another 3D printing technique, selective laser sintering (SLS). SLS produces layer-by-layer materials (no rasters) using polymers or metal powders. More details about FFF and SLS can be found in a study by Ngo et al. [2]. Fig. 2 shows an optical image of the edge view of a carbon fiber–reinforced epoxy IM7/977–3 laminate $[-45/90/45/0]_{3s}$. The average fiber volume percent of the laminate was 68.5 % and different layers were clearly seen.

Fig. 2 also shows a cross-sectional photo of a polymer made with FFF. Three layers had deformed rasters and some voids (dark areas). Usually, fiber-reinforced composites exhibit a high degree of anisotropy in both stiffness and strength and have very high strength and stiffness in the fiber direction, but their stiffness and strength are much smaller in the direction perpendicular to the fibers. Polymers, if made with FFF rasters, are globally isotropic materials because they have no second-phase material. The fiber volume percentage in composites is at least 60 %, so the maximum volume percentage of the matrix is around 40 %, which is much larger than the volume percentage of the voids (<10 %). Therefore, the use of composite laminate theory to characterize the stiffness of 3D printing polymers has significant limitations because it is mainly applicable to polymers with rasters made with FFF.

Generally, 3D printing materials have some anisotropy in their strength, albeit much less than fibrous composites. Therefore, some

* Corresponding author.
E-mail address: l.roy.xu@alumni.caltech.edu (L.R. Xu).

https://doi.org/10.1016/j.compositesa.2024.108288
Received 29 November 2023; Received in revised form 6 May 2024; Accepted 28 May 2024
Available online 29 May 2024

researchers have used composite strength theory to characterize the mixed-mode strengths of FFF polymers (that is, failure due to combined normal and shear stresses). The strength criterion most often used was the Tsai–Hill criterion [3,4], which agreed with some experimental results according to previous papers [5–11]. However, the Tsai–Hill criterion was derived from plasticity theory to predict the yield strength, whereas the experimental data reported in previous papers were the ultimate strengths of FFF polymers. These two strengths were close only when the plasticity was small. In fact, previous researchers usually employed polylactic acid (PLA) as a printing material, which has low plasticity, so it is not surprising that previous experimental results and theoretical predictions agreed well. However, previous mixed-mode strength studies of 3D printing polymers had significant limitations. First, the printing materials were usually limited to one material (PLA), and the 3D printing was limited to one technique (FFF). Second, the Tsai–Hill criterion predicted the yield strength rather than the ultimate strength based on the original Hill's criterion. To predict the ultimate strengths of more 3D printing polymers, composite strength criteria need to be modified to consider the weak anisotropic strengths of 3D printing polymers.

Therefore, this paper presents a systematic experimental and modeling study. In the experiments, both FFF and SLS were employed to make different polymers. The polymer made with SLS had significant plastic deformation, which contradicted the necessary condition for good Tsai–Hill prediction. The polymer made with FFF was used to verify the previous research outcome. Moreover, a new criterion to predict the lower bounds of the ultimate strengths of more 3D printing polymers was employed for comparison with the commonly used Tsai–Hill criterion and maximum stress criterion. From a broader structural safety perspective, using the new criterion to predict the lower bounds of the strengths would yield conservative and safe results. Indeed, we did not pursue a sophisticated strength criterion that would accurately predict the ultimate strengths of all printing polymers, which may be impossible.

2. Theory

2.1. Composite strength criteria versus a new criterion for 3D printing materials

Some sophisticated composite strength criteria were initially based on the theory of plasticity. For an isotropic and homogeneous material subjected to a two-dimensional stress state, the well-known von Mises criterion to predict plastic deformation has the form [3]:

$$\sigma_{1p}^2 + \sigma_{2p}^2 - \sigma_{1p}\sigma_{2p} = \sigma_{yp}^2, \tag{1}$$

where σ_{1p}, σ_{2p}, and σ_{yp} are the principal stresses, and the yield strength was measured from a uniaxial tensile experiment. For a ductile metal with anisotropy, Hill proposed a general criterion for plastic deformation initiation. For a specimen with multiple layers subjected to uniaxial tension, as illustrated in Fig. 3(a), a dashed line represents a 3D printing material layer or a composite layer, and σ_{11}, σ_{22}, and τ_6 are the normal and shear stresses acting on the layer. To develop a new composite strength criterion, Azzi and Tsai [4] modified Hill's criterion for orthotropic composite layers and determined the parameters defined by Hill using imaginary uniaxial experiments. Ultimately, they proposed

$$\left(\frac{\sigma_{11}}{F_1}\right)^2 + \left(\frac{\sigma_{22}}{F_2}\right)^2 + \left(\frac{\tau_6}{F_6}\right)^2 - \left(\frac{\sigma_{11}\sigma_{22}}{F_1^2}\right) = 1, \tag{2}$$

where F_1 is the tensile strength (if $\sigma_{11} > 0$) or compressive strength (if $\sigma_{11} < 0$) in direction 1. For fiber-reinforced composites, direction 1 is the strong fiber direction. F_2 is the tensile strength (if $\sigma_{22} > 0$) or compressive strength (if $\sigma_{22} < 0$) in direction 2, which is perpendicular to direction 1. It should be noted that the orthotropic property assumption (no tension-shear coupling) was employed; otherwise, when $\sigma_{11} > 0$, $\sigma_{22}, \tau_6 \neq 0$. A critical parameter is F_6, which is the in-plane pure shear strength when $\sigma_{11} = \sigma_{22} = 0$. Equation (2) is the Tsai–Hill strength criterion, and it can be employed to predict (1) tensile or compressive failure in directions 1 and 2; (2) in-plane shear failure; and (3) failure under a combined normal and shear stress state. Here failure means the yield strength rather than the ultimate strength based on Hill's original criterion for plastic deformation initiation.

To derive Equation (2), Azzi and Tsai [4] made a major assumption: $F_1 \gg F_2$. This assumption is reasonable for fibrous composites; for example, $F_1/F_2 > 50$ for a typical carbon/epoxy composite [3]. However, this assumption does not hold for all 3D printing materials because the anisotropic degree of the strength of 3D printing materials is usually low. Recently, our experiments on four 3D printing polymers showed that $F_1/F_2 < 4$ [12]. Hence, a simplified criterion to predict the ultimate strengths of 3D printing metals was suggested by the authors [13]:

$$\left(\frac{\sigma_{11}}{F_1}\right)^2 + \left(\frac{\sigma_{22}}{F_2}\right)^2 + \left(\frac{\tau_6}{F_6}\right)^2 = 1. \tag{3}$$

This new criterion was derived based on Hashin and Rotem's composite strength criteria. They assumed that failure of a lamina under a general in-plane loading can be characterized by two failure criteria, one for fiber failure and the other for interfiber failure [3]. The difference between the Tsai–Hill criterion and the new criterion (simplified quadratic criterion) is that the stress interaction item did not show in equation (3). It should be noted that the von Mises criterion has a clear physical meaning—yielding strength. However, equations (2) and (3) are both phenomenological strength criteria that do not have clear physical meanings, but their predicted values agree well with experimental results [14]. Therefore, new experiments were conducted in this study to compare these two strength criteria.

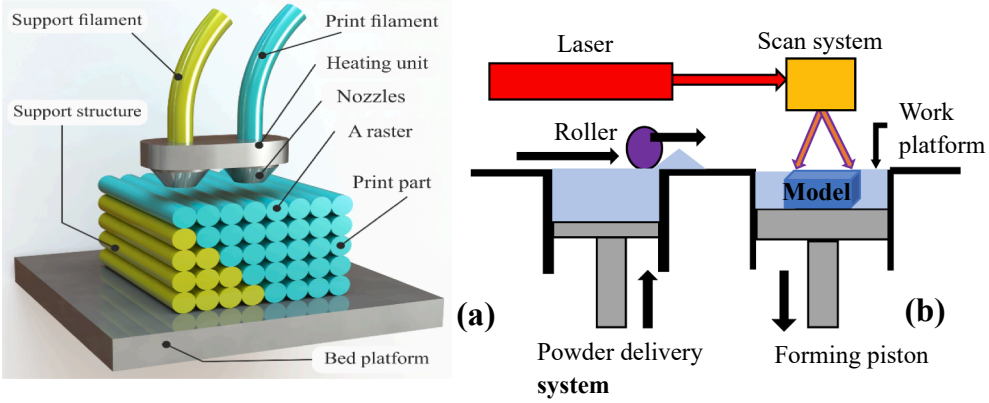

Fig. 1. Illustrations of (a) fused filament fabrication (FFF) by Rahmati et al. [1] and (b) selective laser sintering (SLS).

2.2. Maximum stress criterion for mixed-mode tension strength prediction

Azzi and Tsai [4] conducted extensive tensile experiments on composite laminates with different stacking sequences to validate their criterion. In recent years, similar tensile experiments were extended to 3D printing polymers made with FFF [8–10]. As illustrated in Fig. 3(a), under the uniaxial tensile stress σ, the stresses acting on an element across the interface/printing surface can be obtained using a stress transfer:

$$\sigma_{11} = \sigma cos^2\beta\, \sigma_{22} = \sigma sin^2\beta\, \tau_6 = -\sigma sin\beta cos\beta, \quad (4)$$

where β is the angle between the loading direction and the printing surfaces that bond layers. As the simplest criterion, the maximum composite stress criterion is obtained by equating the above maximum stress components (equation (4)) to the corresponding strengths if σ > 0:

$$F_1 = \sigma cos^2\beta (or \sigma = F_1/cos^2\beta) F_2 = \sigma sin^2\beta F_6 = -\sigma sin\beta cos\beta \quad (5)$$

Usually, a material has a yield strength and an ultimate strength, as illustrated in Fig. 3(b). Only if the plastic deformation is small, the yield strength is close to the ultimate strength [14]. Indeed, the Tsai–Hill criterion should be employed to predict the yield strength because it was extended from the plasticity theory, whereas the maximum stress criterion should be used to predict the ultimate strength. The Tsai–Hill criterion predicted the ultimate strengths of polymeric composite materials and some FFF polymers well because these materials have little plastic deformation, so their yield strengths were close to their ultimate strengths [3,7–10]. In our study, new experiments showed that the Tsai–Hill criterion had limitations in predicting the strengths of ductile polymer specimens. According to Zhang and Xu [13], the quadratic strength criterion provided a conservative lower bound for the strength predictions of 3D printing metals, because its prediction was always lower than the prediction using the Tsai–Hill criterion. This conclusion will be extended to the 3D printing polymers in this study.

3. Materials and methods

3.1. Tensile specimen designs and experiments

Dog-bone specimens, based on international test standard ISO 527-2-2012 (Plastics—Determination of tensile properties, Part 2: Test conditions for molding and extrusion plastics [10]) were employed for the tensile experiments. The reason for choosing this type of specimen was to compare our results with other published results without size effect concern [10]. The specimen size had a length, width, and thickness of 160, 20, and 4 mm, respectively. As shown in Fig. 4, seven kinds of specimens with different build directions were designed. Every 3D printing material had an intrinsic build direction that was perpendicular to the printing surface. However, for the mechanics' analysis, it was convenient to employ the printing surface angle (their difference was 90°). The printing surfaces/interfaces are denoted as dash lines in Fig. 4. The printing surface angle was defined as the angle between the printing surface and the uniaxial loading direction. For example, for specimens with a printing surface angle of 90° (or 90° specimens), the tensile loading was perpendicular to the printing surface (or along the build direction). For each printing surface angle/specimen type, at least eight identical specimens were made, and approximately 80 total specimens were tested. All of the specimens were tested on an Instron 5966 test frame with a 10 kN load cell. The displacement rate was 1 mm/min, and the maximum loadings of the specimens were recorded by the test machine. For some specimens, their strain was measured by a digital image correlation (DIC) VIC-2D system (Correlated Solutions Inc., USA).

3.2. Specimen manufacture using FFF and SLS

Two common types of 3D printing techniques were chosen in order to compare our results with previous results [1,8–10]. For FFF, the PLA filaments were purchased from Shenzhen eSUN Industrial Co., Ltd., China. The filament diameter was 1.75 mm (standard deviation 0.03 mm). The FFF 3D printer was a Raise3D Pro3 (Shanghai Fuzhi Information Technology Co., Ltd., China). The nozzle temperature was 200 °C, the printing speed was 60 mm/s, and the infill degree was 100 %. Other details were reported by Zhang et al. [12]. To manufacture PA specimens using SLS, PA12 powder with a spherical shape and a mean particle size of 120 μm was used, and the apparent density was 0.48 g/cm^3. An SLS apparatus (HT252P, Hunan Farsoon High-Technology Co., Ltd. China) was employed to create the specimens. The apparatus was equipped with a 60 W carbon dioxide laser with a focal laser beam diameter of ≤ 0.5 mm. The processing parameters were determined as a laser power of 45 W, a laser scanning speed of 10 m/s, and a layer thickness of 0.1 mm. Other details were reported by Wang et al. [15].

4. Results and discussion

4.1. Property comparisons of the SLS-PA specimens with different printing surface angles

Fig. 5(a) shows the complete stress–strain curves of seven kinds of typical SLS-PA specimens with printing surface angles of 0° to 90°. A linear loading stage existed for all specimens because they had the same Young's modulus. Also, the initial yielding stage was almost the same for all specimens. As shown in Table 1, their yield strengths were very close. However, their ultimate strengths decreased with the increase of the printing surface angles. To make a further comparison, the properties of our previous injection-molded (IM) PA specimens [12] are also listed in Table 1. The IM-PA specimens had the same Young's modulus as the SLS-PA specimens, but very different yield and ultimate strengths. It is noted that the standard deviations of the IM-PA specimens were much smaller than the standard deviations of the printing PA specimens because more initial defects could be introduced during the 3D printing process. Fig. 5(b) shows the load–displacement curves of all the 0° specimens, and the same linearly elastic deformation stage can be clearly seen.

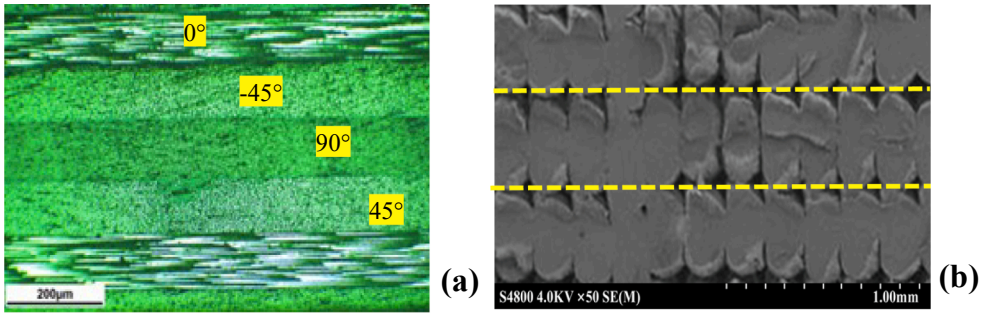

Fig. 2. Cross-sectional views of (a) fibers/matrix layers in composites and (b) rasters in specimens made with FFF.

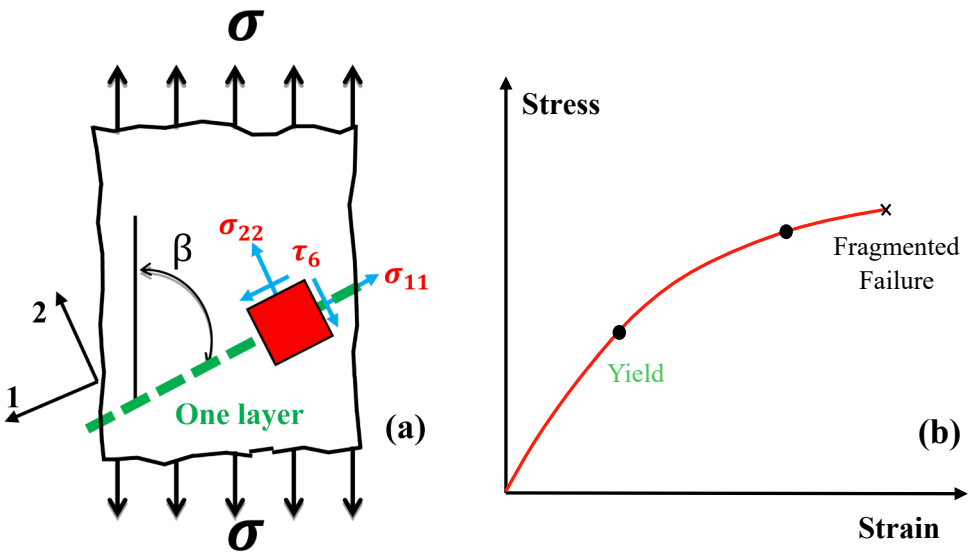

Fig. 3. (a) Stress distributions at an interface in a 3D printing polymer or a composite laminate subjected to uniaxial tension, and (b) its failure process [13].

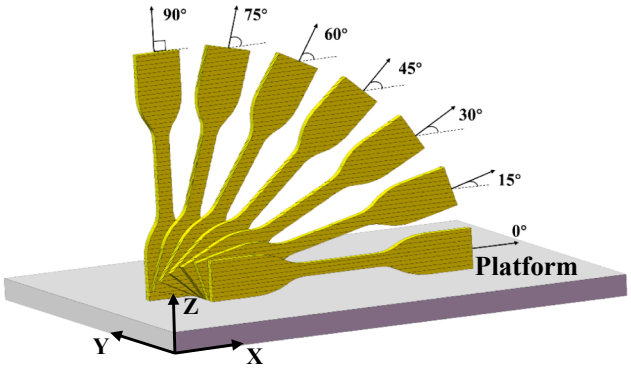

Fig. 4. Specimens with different printing surface angles in this study.

4.2. Special dynamic crack branching phenomenon of the SLS-PA specimens

Fig. 6 shows the photos of all fractured 0° specimens, which had a consistent fracture pattern of crack branching, i.e., after one main crack initiated from the specimen's edge, it became two branching cracks, which then penetrated the whole specimen width. Crack branching has been a challenging topic in the study of dynamic fracture for the past 70 years [16]. According to the most recent experimental work of Xu and Rosakis on crack branching in brittle polymers [17], the crack branching phenomenon we observed has never before been reported in 3D printing materials, so it requires further investigation. In this section, we not only explain the common aspects of crack branching but also highlight its new features in a 3D printing polymer (SLS-PA). In almost all previous crack branching experiments, the specimens were subjected to dynamic loading such that the cracks had enough speed for branching [18], because the first factor of crack branching is the crack speed. Under the mode-I loading condition, one main/mother crack yields two branching/daughter cracks. Based on high-speed photography [17], all branching cracks are symmetrical mode-I cracks. However, crack branching in our experiments occurred during the static tension experiments, so the main crack speed was not high although the speed was not measured.

The second factor of crack branching was related to the crack energy release. A crack has high potential energy, so it breaks the material and release energy out by creating fracture surfaces. If the main crack has a large amount of potential energy to release (a dynamic crack has no kinetic energy), crack branching may occur, thus creating more fractured surfaces and releasing more energy. This was supported by our tension experiments. The tensile load–displacement curves of the 90° specimens are shown in Fig. 7. Compared to Fig. 5(b) for the 0° specimens, the work done by the external force (the area under the load–displacement curve) for the 90° specimens was much less than that

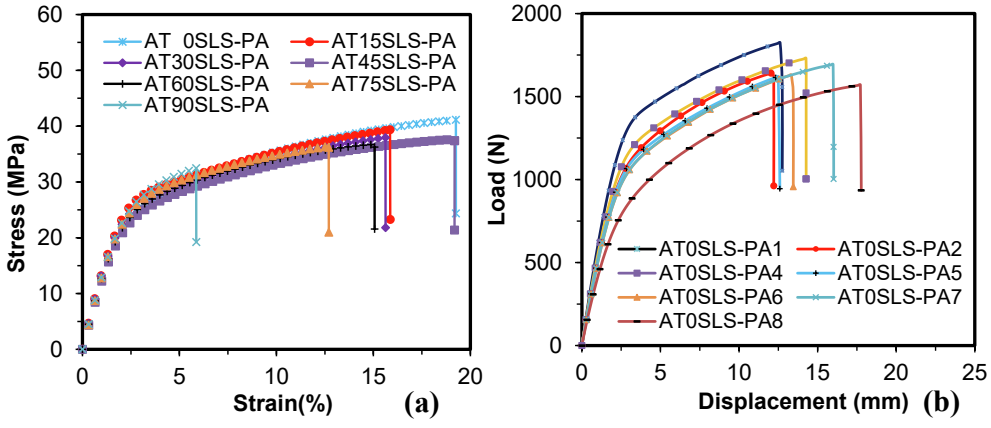

Fig. 5. (a) Stress–strain curves of all typical SLS-PA specimens and (b) force–displacement curves of the 0° specimens.

Table 1
Mechanical properties of PA specimens as a function of the printing surface angles and the strength predictions using two criteria.

Specimen	Young's modulus (GPa)	Yield strength (MPa)	Ultimate strength (MPa)	Tsai–Hill criterion prediction (MPa)	Quadratic criterion prediction (MPa)	Crack branching angle Ω
Inject-molded	1.37 ± 0.01	35.11 ± 0.82	43.63 ± 0.27			
SLS-0°	1.32 ± 0.06	17.83 ± 0.96	41.04 ± 1.98	41.04	41.04	42.9°
SLS-15°	1.31 ± 0.04	18.96 ± 0.23	40.09 ± 3.32	41.16	39.93	39.3°
SLS-30°	1.23 ± 0.13	18.18 ± 1.13	37.49 ± 2.38	40.89	37.55	34.1°
SLS-45°	1.28 ± 0.11	17.72 ± 1.15	38.73 ± 1.06	39.21	35.38	32.6°
SLS-60°	1.28 ± 0.05	17.79 ± 0.86	35.42 ± 2.58	36.49	34.05	32.1°
SLS-75°	1.26 ± 0.05	17.64 ± 1.26	34.47 ± 1.78	34.20	33.48	31.3°
SLS-90°	1.34 ± 0.06	18.95 ± 0.75	33.34 ± 2.10	33.34	33.34	0°

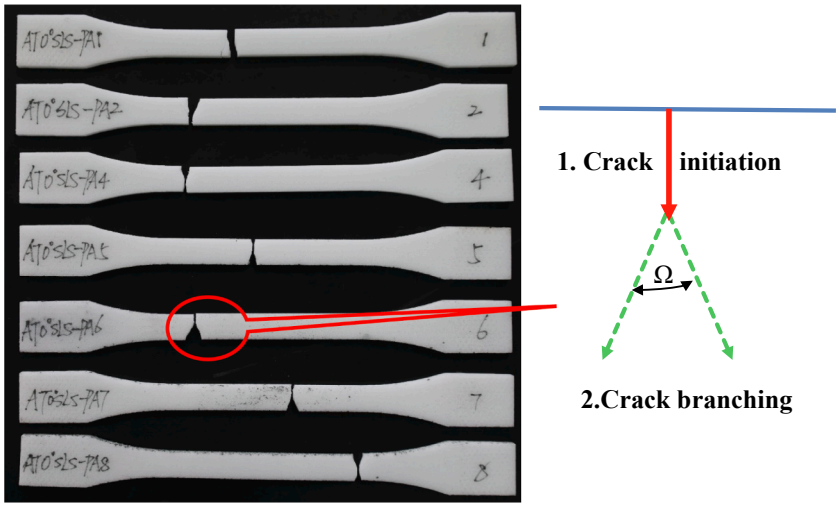

Fig. 6. Crack branching photos of all 0° specimens of SLS-PA. The main crack initiated from one specimen and then branched into two cracks and penetrated the specimen width.

of the 0° specimens. Therefore, it was not surprising to see that all 90° specimens had less potential energy and no crack branching, i.e., the specimen failed as one crack that penetrated the specimen width. For some specimens, it was interesting to find that the main crack propagated along the interface first, and then one branching crack propagated along the same interface as well, as shown in Fig. 8. However, these events only occurred for the printing surface angles of 60° and 75°. Another unique phenomenon was that the main crack branched into three cracks in some cases. Furthermore, the theoretical maximum crack branching angle was 55° [16,17]; the crack branching angles shown in Table 1 did not exceed this limit and decreased with the increase of the printing surface angles. Notably, there were two different mechanics topics for the failure of all SLS-PA specimens: 1) initial failure from the edge, i.e., a strength problem (no initial crack); and 2) crack branching as the final failure, i.e., a fracture problem (with an initial crack from the specimen edge).

Crack branching is often explained by dynamic fracture mechanics. According to Freund [16], crack branching generally occurs only at a high crack tip speed that is most often larger than one-fifth of the Rayleigh wave speed of the material with a crack. To understand complicated crack branching, the hoop stress (tensile stress in the θ-direction) near the tip of a steady mode-I main crack in a polar coordinate system was given by Freund [16]:

$$\sigma_h(r,\theta,t) = \frac{K_I(t)}{\sqrt{2\pi r}}\Sigma_h^I(\theta,v) \tag{6}$$

where $K_I(t)$ is the dynamic stress intensity factor of the mode-I main crack as a function of time t; the function of $\Sigma_h^I(\theta,v)$ represents the angular variations of the stress components of the main crack with a tip speed v. The normalized hoop stress is plotted in Fig. 9 as a function of the normalized crack tip speed v/c_s (c_s is the shear wave speed of the material). It is clearly seen that the peak values of the hoop stresses, which lead to crack branching, increase as the normalized crack tip speed increases. It is clear that a static crack or a crack with a low speed cannot have any branching trend. However, in our experiments, crack branching appeared when the static loading rate was 1 mm/min. According to equation (6), if the main crack reaches around 856 m/s (0.8 v/c_s), it will branch. We believe that all crack speeds in our static tension experiments were far below this crack speed based on our extensive high-speed photography of dynamic fracture [17]. Due to the difficulty in dynamic fracture mechanics modeling for crack branching, we mainly present some interesting experimental phenomena rather than modeling. Indeed, new crack branching criteria should be proposed because previous mechanics factors, such as the crack speed and energy release, were not sufficient. Moreover, the same PA specimens made with FFF did not have any crack branching during static tension failure in our recent experiments [12]. Therefore, mechanics as well as material factors are necessary for future crack branching modeling. However, a similar fracture phenomenon in 3D printing polymers, crack kinking (one main crack changes its propagation direction) [19], can be modeled using fracture mechanics theory [20].

4.3. Ultimate strength prediction and the lower bound prediction of ultimate strengths

Figs. 10 and 11 show the comparisons of our tensile strength measurements of all SLS-PA specimens with the predictions of the original

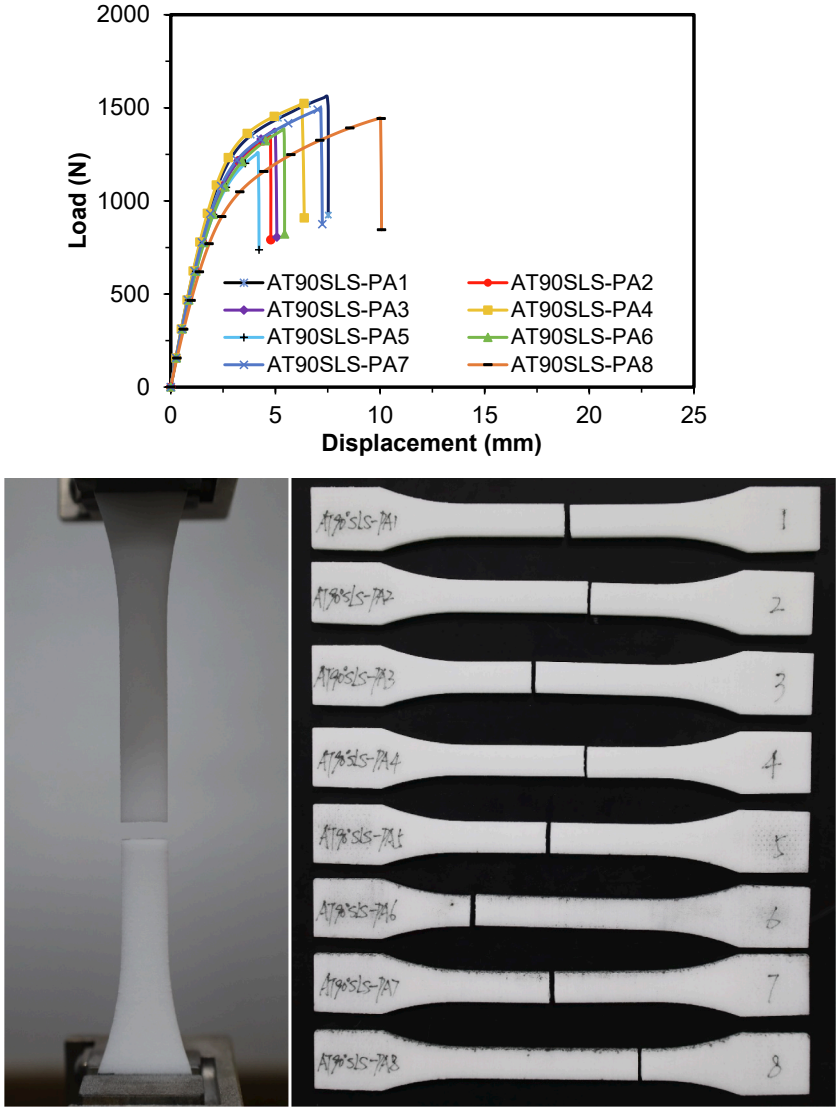

Fig. 7. Force-displacement curves of all 90° specimens of SLS-PA and their final failure patterns without any crack branching.

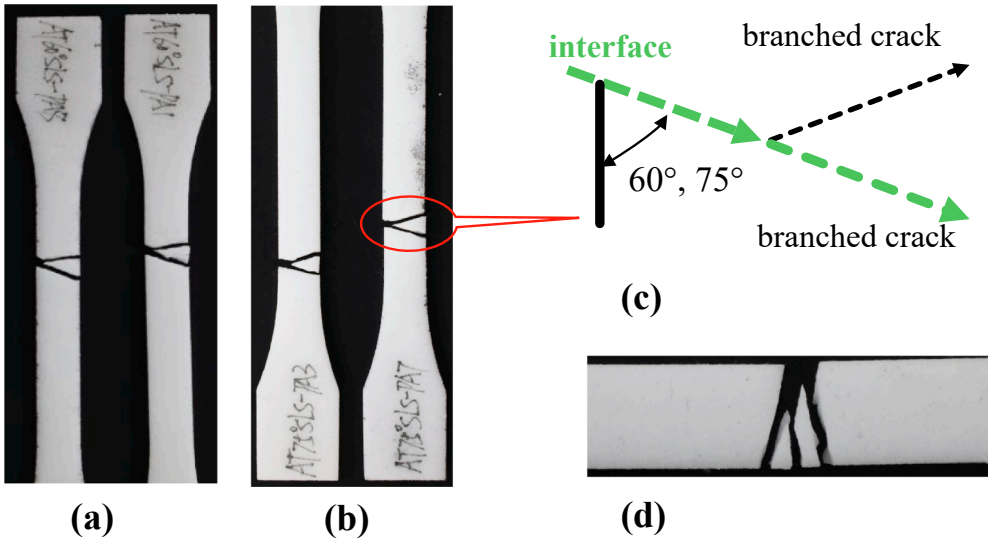

Fig. 8. Special crack branching of the other SLS-PA specimens: (a) and (b) inside specimens with the printing surface angles of 60° and 75°; (c) the main crack propagated along the interface and then one branched crack propagated along the interface; (d), the main crack branched into three cracks in some cases.

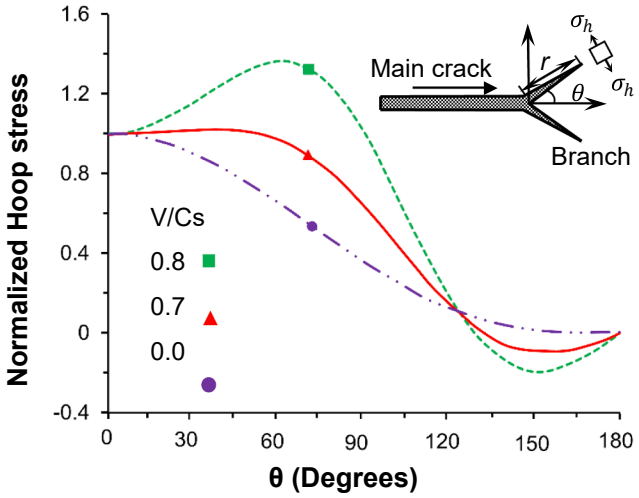

Fig. 9. Normalized dynamic hoop stress variation of a dynamic main crack as a function of the crack tip speed (Freund 1990).

and simplified maximum stress criteria [3], the Tsai–Hill criterion, and the new quadratic criterion. These material properties were employed in the predictions for $F_1 = 41.04$ MPa, $F_2 = 33.34$ MPa ($F_1/F_2 < 1.5$), and $F_6 = 24.24$ MPa, which were based on our own shear strength measurement for the same SLS-PA material system in this study [15]. The original maximum stress criterion yielded bizarre results, and its predicted strengths were much larger than the measured strengths. The simplified maximum stress criterion mainly drooped the shear strength [3] and yielded the upper bound prediction of the tensile ultimate strengths, but the upper bound of the strengths was not right for safety. The prediction using the Tsai–Hill criterion generally overestimated the measured strengths, and it was not as accurate as the results reported in previous papers for brittle FFF specimens [8–10]. However, the prediction using the quadratic criterion was often below the measured strengths. Therefore, it is more appropriate to define the quadratic criterion prediction as the lower bound prediction. As expected, the prediction using the Tsai–Hill criterion was always higher than that using the quadratic criterion, so it is not safe for future applications. The calculation error of the Tsai–Hill criterion was due to its inaccurate assumption that $F_1 \gg F_2$ for 3D printing polymers.

Fig. 12 shows our strength data of the FFF-PLA specimens using 5 and 10 % fan-power (fan-power is the rated power of a cooling fan,

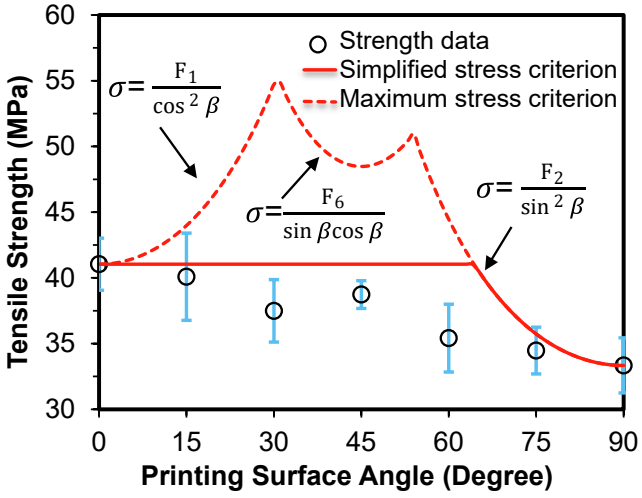

Fig. 10. Comparisons of the tensile strength measurements of the SLS-PA specimens with the original and simplified maximum stress criteria.

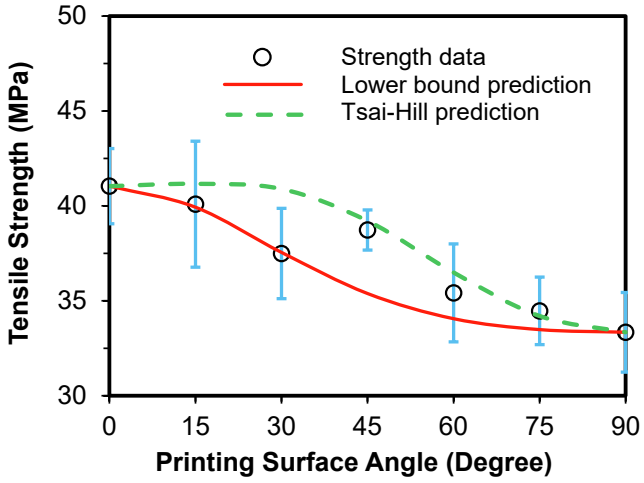

Fig. 11. Comparisons of the tensile strength measurements of the SLS-PA specimens with the Tsai–Hill and the quadratic criteria.

which is an important process parameter for FFF printing). The predictions using the quadratic criterion (shear strength 25.74 MPa based on our own measurement) were always higher than the measured strengths. Of course, the Tsai–Hill predictions would be even higher, so they are not shown in Fig. 12. Based on the results of our two kinds of 3D printing materials (SLS-PA and FFF-PLA), it might not be possible to propose a criterion that can accurately predict the ultimate strengths of all 3D printing polymers.

To validate the quadratic criterion prediction as the lower bound prediction, in addition to our own SLS and FFF specimens, comparisons of the material systems reported in other papers are presented in Figs. 13–15. Zhao et al. [8] measured the strengths of FFF-PLA specimens with two printing layer thicknesses of 0.1 and 0.3 mm, and the quadratic criterion primarily predicted the lower bound shown in Fig. 13. Fig. 14 shows the strength measurements of another FFF-PLA material system reported by Yao et al. [9]. The above results were exactly repeated. Moreover, the same outcome appeared for another FFF-PLA material system reported by Yao et al. [10]. Because we only cited their data without their standard deviations, the quadratic criterion for the lower bound prediction of the ultimate strengths looks applicable to most 3D printing polymers, in addition to being more conservative than the Tsai–Hill criterion. Indeed, the previous papers

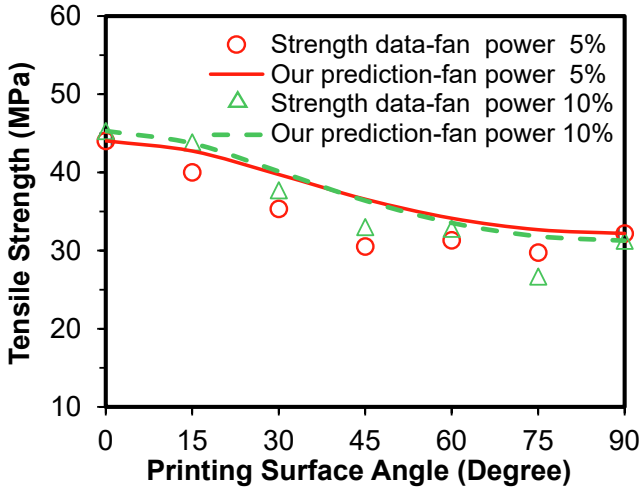

Fig. 12. Our tensile strength measurements of FFF-PLA specimens using 5 % and 10 % fan-power (the rated power of the cooling fan) and our prediction using the quadratic criteria (shear strength 25.74M Pa).

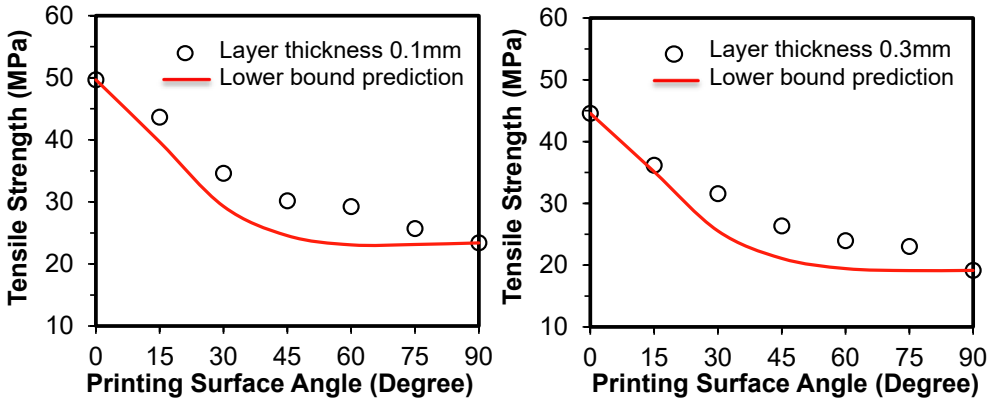

Fig. 13. Comparisons of the lower bound predictions of the ultimate strengths with the strength measurements of FFF-PLA specimens with different layer thicknesses reported by Zhao et al. [8].

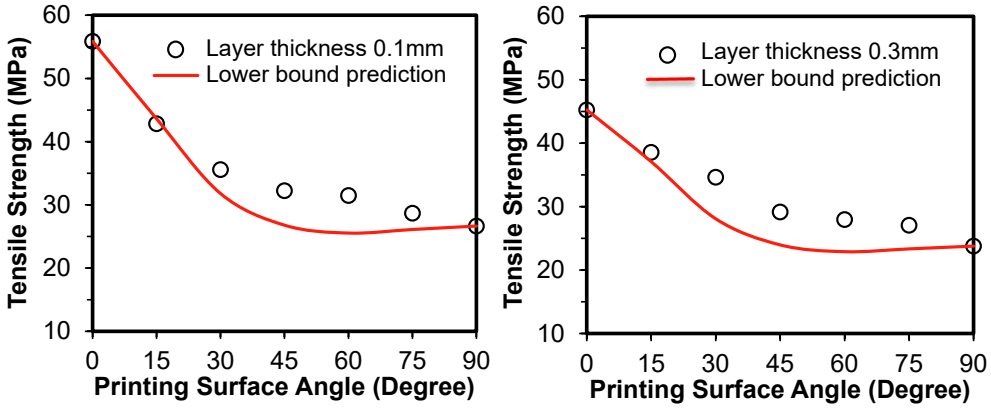

Fig. 14. The lower bound predictions of the ultimate strengths and the strength measurements of FFF-PLA specimens with different layer thicknesses reported by Yao et al. [9].

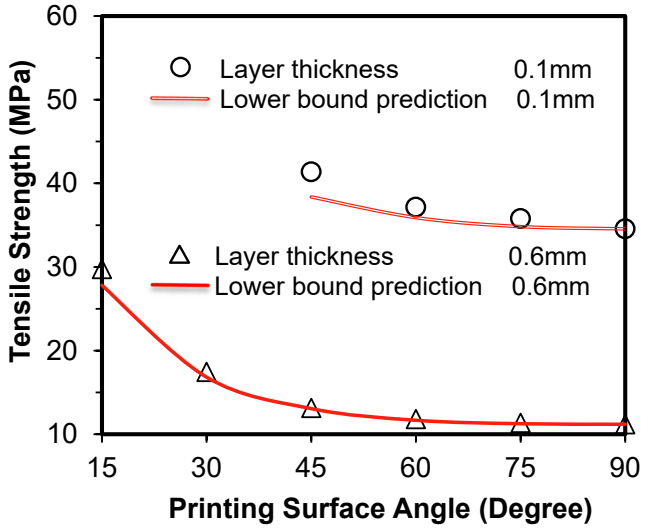

Fig. 15. The lower bound predictions of the ultimate strengths and the strength measurements of FFF-PLA specimens with different layer thicknesses reported by Yao et al. [10].

only focused on one FFF-PLA polymer that had little plastic deformation. Furthermore, the Tsai–Hill criterion requires the shear strength as an important parameter for accurate predictions. However, this parameter was only assumed (not measured) in all previous papers, so the Tsai–Hill criterion accurately predicted the ultimate strengths in previous papers even though this criterion should be used to predict the yield strength based on Hill's original criterion. In our experiments, we measured the critical shear strength for the same material system and found that the Tsai–Hill criterion was limited.

As reported by the authors, the quadratic criterion was employed for predicting the lower bounds of the ultimate strengths of several 3D printing metals that are available in the open literature [13]. Thus, the quadratic criterion could be extended to more 3D printing materials. The composite strength criteria, such as the Tsai–Hill criterion and the maximum stress criterion, did not predict the ultimate strengths of 3D printing polymers and metals well, because they are intended to be used to predict the composite strengths with strong anisotropic degrees, whereas the above 3D printing materials (single-material printing) only have strengths with weak anisotropic degrees.

In recent years, 3D printing composite materials have become a major research direction [21–25], and existing strength criteria may not apply to these materials because of their strong anisotropic mechanical properties and complicated material configurations. Some researchers found that, similarly to fiber orientations, different raster orientations affect the ultimate strength of polymers made with FFF [26]. However, it is important to note that the raster orientations inside a layer are only applicable to materials made with FFF, whereas our efforts were focused on a broader range of 3D printing materials.

Based on the two failure modes in this study, i.e., tensile strength failure and crack propagation/branching, pure strength research is not enough for 3D printing materials. Fracture mechanics research should become the priority as demonstrated in recent publications [21,27–29].

Usually, materials are subjected to applied normal and shear stresses, therefore, mixed-mode fracture research of 3D printing materials [28,29] is more important than the common mode-I fracture research.

5. Conclusion

Existing composite strength criteria are unable to correctly predict the ultimate strengths of all 3D printing polymers. For example, the Tsai–Hill criterion was originally based on plasticity theory because it was intended to predict the yield strengths of brittle composite materials with high anisotropic strengths, but many 3D printing polymers are plastic and have weak anisotropic strengths. Our proposed quadratic strength criterion provided conservative strength-bound predictions to ensure safety. To our knowledge, this was the first study to observe dynamic crack branching in 3D printing specimens under static tension. This dynamic crack branching followed some previous crack branching rules but also presented new behavior, such as crack branching of a slow main crack. These novel results bring new challenges to theory and simulations. Therefore, the strength/failure of 3D printing polymers becomes more complicated than that of the original bulk polymers. Future research directions should include new crack branching criteria with the material factors and modified ultimate strength criteria for 3D printing composite laminates.

CRediT authorship contribution statement

Gonghe Zhang: Writing – original draft, Visualization, Validation, Methodology, Investigation, Formal analysis. **Xiaodong Zheng:** . **Qinglin Wang:** . **Yinxu Ni:** . **Fenghua Liu:** . **Kai Zhao:** . **Luoyu Roy Xu:** Writing – review & editing, Supervision, Project administration, Methodology, Investigation, Formal analysis, Conceptualization.

Declaration of competing interest

The authors declare that they have no known competing financial interests or personal relationships that could have appeared to influence the work reported in this paper.

Data availability

Data will be made available on request.

References

[1] Rahmati A, Heidari-Rarani M, Lessard L. A novel conservative failure model for the fused deposition modeling of polylactic acid specimens. Addit Manuf 2021;48:102460.
[2] Ngo T, Kashani A, Imbalzano G, Nguyen K, Hui D. Additive manufacturing (3D printing): a review of materials, methods, applications and challenges. Compos Part B Eng 2018;143:172–96.
[3] Daniel IM, Ishai O. Engineering Mechanics of Composite Materials. New York: Oxford University Press; 2005.
[4] Azzi VD, Tsai SW. Anisotropic strength of composites. Exp Mech 1965;5(9):283.
[5] Mustafa Güden H, Yava AAT, et al. Orientation dependent tensile properties of a selective-laser-melt 316L stainless steel. Mater Sci Eng, A 2021;824:141808.
[6] Domingo-Espin M, Puigoriol-Forcada JM, Garcia-Granada A-A, et al. Mechanical property characterization and simulation of fused deposition modeling polycarbonate parts. Mater Des 2015;83:670–7.
[7] Zou R, Xia Y, Liu S, Hu P, Hou W, Hu Q, et al. Isotropic and anisotropic elasticity and yielding of 3D printed material. Compos Part B Eng 2016;99:506–13.
[8] Zhao Y, Chen Y, Zhou Y. Novel mechanical models of tensile strength and elastic property of FDM AM PLA materials: experimental and theoretical analyses. Mater Des 2019;181:108089.
[9] Yao T, Deng Z, Zhang K, Li S. A method to predict the ultimate tensile strength of 3D printing polylactic acid (PLA) materials with different printing orientations. Compos Part B Eng 2019;163:393–402.
[10] Yao T, Zhang K, Deng Z, Ye J. A novel generalized stress invariant-based strength model for inter-layer failure of FFF 3D printing PLA material. Mater Des 2020;193:108799.
[11] Alaimo G, Marconi S, Costato L, Auricchio F. Influence of meso-structure and chemical composition on FDM 3D-printed parts. Compos Part B Eng 2017;113:371–80.
[12] Zhang G, Wang Q, Ni Y, Liu P, Liu F, Leguillon D, et al. A systematic investigation on the minimum tensile strengths and size effects of 3D printing polymers. Polym Test 2023;117:107845.
[13] Zhang G, Xu LR. Simplified criterion to predict the lower bounds of the anisotropic ultimate strengths of 3D printing metals. Eng Fail Anal 2023;149:107240.
[14] Christensen RM. Theory of Materials Failure; Oxford Univ. Oxford, UK: Press; 2013.
[15] Wang Q, Zhang G, Zheng X, Liu Y, Xu LR. Efficient characterization on the interlayer shear strengths of 3D printing polymers. J Mater Res Technol 2023;22:2768–80.
[16] Freund LB. Dynamic Fracture Mechanics. New York: Cambridge University Press; 1990.
[17] Xu LR, Rosakis AJ. Real-time experimental investigation of dynamic crack branching using high-speed optical diagnostics. Exp Tech 2003;27:23–6.
[18] Ravi-Chandar K, Knauss W. An experimental investigation into dynamic fracture: III. On steady-state crack propagation and crack branching. Int J Fract 1984;26:141–54.
[19] Ameri B, Taheri-Behrooz F, Aliha MRM. Evaluation of the geometrical discontinuity effect on mixed-mode I/II fracture load of FDM 3D-printed parts. Theor Appl Fract Mech 2021;113:102953.
[20] Zehnder AT. Fracture Mechanics. Netherlands: Springer; 2012.
[21] Yavas D, Zhang Z, Liu Q, Wu D. Fracture behavior of 3D printed carbon fiber-reinforced polymer composites. Compos Sci Technol 2021;208:108741.
[22] Das M, Mishra R, Das P, et al. Controlled directionality in 3D printing of graphite-reinforced polymer composite with enhanced mechanical properties. Compos Sci Technol 2023;235:109955.
[23] van de Werken N, Hurley J, Khanbolouki P, Sarvestani AN, Tamijani AY, Tehrani M. Design considerations and modeling of fiber reinforced 3D printed parts. Compos Part B Eng 2019;60:684–92.
[24] Chen Y, Ye L. Designing and tailoring effective elastic modulus and negative Poisson's ratio with continuous carbon fibres using 3D printing. Compos Part A Appl Sci Manuf 2021;150:106625.
[25] Z. Zhang, Yu Long, Zhe Yang, Kunkun Fu, Yan Li. An investigation into printing pressure of 3D printed continuous carbon fiber reinforced composites. Compos. Part A Appl Sci Manuf., 162 (2022) 107162.
[26] Khosravani MR, Berto F, Ayatollahi MR, et al. Characterization of 3D-printed PLA parts with different raster orientations and printing speeds. Sci Rep 2022;12:1016.
[27] Bragaglia M, Cecchini F, Paleari L, Ferrara M, Rinaldi M, Nanni F. Modeling the fracture behavior of 3D-printed PLA as a laminate composite: influence of printing parameters on failure and mechanical properties. Compos Struct 2023;322:117379.
[28] Khosravani MR, Rezaei S, Ruan H, Reinicke T. Fracture behavior of anisotropic 3D-printed parts: experiments and numerical simulations. J Mater Res Technol 2022;19:1260–70.
[29] Ameri B, Taheri-Behrooz F, Aliha MRM. Mixed-mode tensile/shear fracture of the additively manufactured components under dynamic and static loads. Eng Fract Mech 2022;260:108185.